

Three-body interactions on a triangular lattice

Xue-Feng Zhang,^{1,2,*} Yu-Chuan Wen,³ and Yue Yu¹

¹*Institute of Theoretical Physics, Chinese Academy of Sciences, P.O. Box 2735, Beijing 100190, China*

²*Physics Department and Research Center OPTIMAS, University of Kaiserslautern, 67663 Kaiserslautern, Germany*

³*Center of Theoretical Physics, Department of Physics, Capital Normal University, Beijing 100048, China*

(Dated:)

We analyze the hard-core Bose-Hubbard model with both the three-body and nearest neighbor repulsions on the triangular lattice. The phase diagram is achieved by means of the semi-classical approximation and the quantum Monte Carlo simulation. For a system with only the three-body interactions, both the supersolid phase and one third solid disappear while the two thirds solid stably exists. As the thermal behavior of the bosons with nearest neighbor repulsion, the solid and the superfluid undergo the 3-state Potts and the Kosterlitz-Thouless type phase transitions, respectively. In a system with both the frustrated nearest neighbor two-body and three-body interactions, the supersolid and one third solid revive. By tuning the strength of the three-body interactions, the phase diagram is distorted, because the one-third solid and the supersolid are suppressed.

PACS numbers: 05.30.Jp, 03.75.Hh, 03.75.Lm, 75.40.Mg, 75.10.Jm

I. INTRODUCTION

While it is an adjustable quantum simulator for solving some difficult quantum problems, such as the high- T_c superconductivity and the fractional quantum Hall effects, the system of the ultracold molecules trapped in the optical lattice also provides an ideal toolbox to analyze the general properties of the quantum many-body systems¹⁻³. In the real materials, comparing with the dominant role that the two-body interactions play, the multi-body interactions are usually taken as the high-order perturbation. On the other hand, the man-made Hamiltonian with leading multi-body interactions exhibits many distinctive phenomena, such as the non-abelian topological phases⁴ and several novel phases⁵⁻⁷ originated from the ring exchange interactions. Recently, because of the engineering development of the ultracold polar molecules confined in the optical lattice, the multi-body interactions can be experimentally realized, especially, the three-body interactions can be varied in a wide range with the nearest neighbor interactions from negative to positive⁸.

While the dominant three-body interactions result in many exotic phases⁹⁻¹² on one-dimensional chains and two-dimensional bipartite lattices, the interplay between the three-body interactions and the geometry frustration is still unclear. The frustrated lattices (such as the triangular and Kagome lattices) manifest themselves by enhancing the quantum fluctuation and often accompanying with the highly degenerate ground state. In the magnetic materials with the triangular structure, the spin liquid which breaks no symmetry has been observed¹³. Meanwhile, the triangular optical lattice, in which the existence of the supersolid has been numerically proved¹⁴⁻²¹, has been realized by using triple laser beams^{22,23}.

The simplest model to reflect such an interplay is the

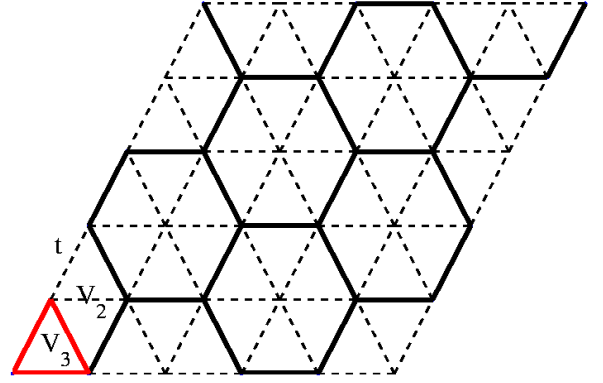


FIG. 1: (Color online) The hard-core Bose Hubbard Model on the triangular lattice. The particles can hop on the bond with amplitude t , and the nearest neighbor repulsion V_2 exists between them. The three-body interactions V_3 affect the particles on the triangle marked by red thick lines. In the $2/3(1/3)$ solid, the particles(holes) will occupy two sublattices (black thick line) and form the honeycomb backbone.

hard-core bosons with nearest neighbor two-body and three-body repulsions on the triangular lattice. The Hamiltonian in the grand canonical ensemble is shown in Fig.1 and given

$$H = -t \sum_{\langle ij \rangle} (b_i^\dagger b_j + b_j^\dagger b_i) + V_2 \sum_{\langle ij \rangle} n_i n_j - \mu \sum_i n_i + V_3 \sum_{\langle i,j,k \in \Delta \rangle} n_i n_j n_k, \quad (1)$$

where b_i^\dagger (b_i) is the creation (annihilation) operator of bosons; t is the hopping parameter; μ is the chemical potential; and V_2 and V_3 are strengths of the nearest neighbor two-body and three-body repulsions, respec-

tively, i.e., $\langle i, j \rangle$ represents i and j are nearest neighbor sites and $\langle i, j, k \in \Delta \rangle$ means i, j and k connect with each other two by two and form a regular triangle. After the Holstein-Primakoff transformation $b_i^\dagger \rightarrow S_i^\dagger$, $b_i \rightarrow S_i$ and $n_i \rightarrow S_i^Z + 1/2$, the bosonic Hamiltonian (1) is mapped into spin-1/2 XXZ model

$$H = -t \sum_{\langle ij \rangle} (S_i^\dagger S_j + S_j^\dagger S_i) + (V_2 + V_3) \sum_{\langle ij \rangle} S_i^Z S_j^Z - B \sum_i S_i^Z + V_3 \sum_{\langle i, j, k \in \Delta \rangle} S_i^Z S_j^Z S_k^Z, \quad (2)$$

where $B = \mu - 3V_2 - 3V_3/2$, and the last term breaks the particle-hole symmetry.

In this work, we used both the semi-classical approximation¹⁴ and quantum Monte Carlo simulation²⁴⁻²⁶ to study the model described by the Hamiltonian Eq. (2). We first assume $V_2 = 0$ and merely consider the three-body interactions. We depict the phase diagram and find the coexistence of both the charge-density wave order and the bond-ordered wave⁹. Furthermore, at the finite temperature, the Kosterlitz-Thouless and the 3-state Potts type phase transitions are found in the superfluid phase and the solid phase, respectively. After the antiferromagnetic nearest neighbor interaction is switched on, the phase diagram is derived in the whole parameter space. For the large three-body interactions, we observe the separation of the minima of the superfluid density and the structure factor.

II. THREE-BODY INTERACTIONS

In Refs. [14,15], the authors showed that the frustrated nearest neighbor interaction leads to the charge density wave (CDW) order. In this section, we show that the three-body interactions play the same role as the nearest neighbor interaction does.

When the hopping is forbidden, i.e., $t = 0$, the ground state at the absolute zero temperature is exactly known. All the sites are empty (Mott-0 Insulator) when μ is less than 0. As the chemical potential increases, a $\sqrt{3} \times \sqrt{3}$ solid phase appears in order to maximize the chemical potential part without costing energy on the three-body repulsions. When $\mu > 6V_3$, the system is fully occupied (Mott-1 Insulator), because the energy paid in the three-body interactions is less than its gain from the chemical potential. For a finite t there may be a superfluid phase. Then, the phase diagram is extended to the finite t and shown in Fig.2.

A. Semi-classical approximation

By approximating the quantum spin in Eq. (2) as a classical unit vector with the magnitude 1/2, the system

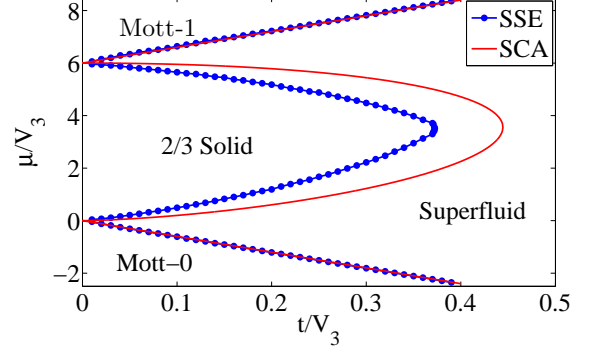


FIG. 2: (Color online) The phase diagram with $V_2 = 0$. The red line comes from the semi-classical approximation (SCA) and the dot blue line from quantum Monte Carlo with a stochastic series expansion (SSE) arithmetic.

is taken the semi-classical approximation. The ground state is determined by minimizing the energy per site. Because of the 3-fold rotational and the translational symmetries, the lattice can be divided into three sublattices, and the spins are equivalent in each one.

The superfluid is classically identified by checking whether all the spins point at the same direction. By using the semi-classical approximation, we find that the second order Mott-0(Mott-1) insulator-superfluid phase transition at $h = -2\Delta$ ($h = 2(2+\Delta)$), where $\Delta = 2t/V_3$ and $h = 2\mu/3V_3$. Meanwhile, the phase transition between solid and superfluid state is the first order, and the critical lines can be analytically expressed with

$$h = \frac{16 - 3\Delta^2}{12} + \frac{c^{1/3} \cos((\theta - 2\pi)/3)}{6} \quad (3)$$

and

$$h = \frac{16 - 3\Delta^2}{12} + \frac{c^{1/3} \cos(\theta/3)}{6}, \quad (4)$$

where

$$\begin{aligned} a &= 4096 - 2304\Delta^2 - 5760\Delta^3 - 2160\Delta^4 \\ &\quad - 216\Delta^5 - 27\Delta^6 \\ b &= \sqrt{c^2 - a^2} = 48\sqrt{6\Delta^3(8 - 9\Delta)(8 + 4\Delta + \Delta^2)} \\ c &= (256 - 96\Delta^2 + 48\Delta^3 + 9\Delta^4)^{3/2} \\ \theta &= \arccos(a/c). \end{aligned}$$

And the summit of the lobe is at $\Delta = 8/9$ and $h = 64/27$, which is given by equalizing Eq. (3) and Eq. (4) at $\theta = \pi$. The peak and the shape of the lobe in the Fig.2 also reflect the breaking of the particle-hole symmetry. Notice that the semi-classical approximation is exact in the large-S limit and the result from this approximation is only qualitatively correct. To depict the precise phase diagram, we use a stochastic series expansion (SSE) arithmetic in quantum Monte Carlo simulation.

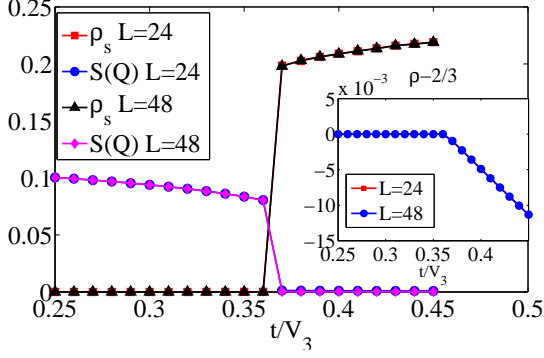


FIG. 3: (Color online) The structure factor and the superfluid density (Inset: The density per site) at $\mu/V_3 = 3.5$ and $T = 0.01V_3$ vs t/V_3 . L is the linear size of the lattice.

B. Quantum Monte Carlo

The cluster SSE^{24–26} is taken because of its high accuracy and efficiency on simulating the system with the multi-body interactions. The sufficiently low temperature and large system size ensure the thermodynamic limit to be achieved, and the number of the quantum Monte Carlo steps are up to one million. A solid phase may be described by a charge density wave (CDW) order parameter, the structure factor $S(\mathbf{Q}) = \langle |\sum_{k=1}^N n_k e^{i\mathbf{Q} \cdot \mathbf{r}_k}|^2 \rangle / N^2$ where N is the number of sites and $\mathbf{Q} = (4/3\pi, 0)$. Meanwhile, the long range off-diagonal order is reflected by the finite superfluid density $\rho_s = \langle W^2 / 4\beta t \rangle$, where W is the winding number. In the $2/3$ filling CDW state, the bosons fully occupy two sublattices, so that the particle and hole on same bond can partly form a singlet state due to the second order hopping process. Thus, the bond order wave appears. It is described by the non-zero bond order structure factor $S_b(\mathbf{Q}) = \langle |\sum_{l=1}^{N_b} K_l e^{i\mathbf{Q} \cdot \mathbf{r}_l}|^2 \rangle / N^2$, where N_b is the number of bonds, $K_l = b_i^\dagger b_j + b_j^\dagger b_i$ and i, j are two ends of the bond l .

In the inset of the Fig.3, the density plateau indicates the incompressible state. And in the Fig.3, the finite values of the $S(\mathbf{Q})$ and zero superfluid density in the left part (small t/V_3) support the existence of the solid state ($\rho = 2/3$) in this region. Meanwhile, the finite jump of the superfluid density and zero $S(\mathbf{Q})$ in the right part indicate the first order superfluid-solid phase transition at the critical point $t/V = 0.36(1)$. The $S_b(\mathbf{Q})$ also drops down at the same critical point, as shown in the Fig.4. However, the dependence on the lattice size requires the finite size scaling analysis, which is shown in Fig.5. We see that the system has a finite bond order wave order in the solid phase and not in the superfluid. Thus, we confirmed that the bond order wave and CDW coexist in the solid and do not separate. However, it is not a novel phase because it can be easily understood by the local vibrations of the particles or holes. The inset of the

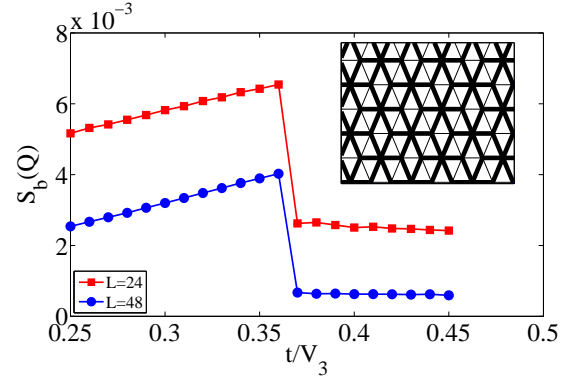


FIG. 4: (Color online) The $S_b(\mathbf{Q})$ at $\mu/V_3 = 3.5$ and $T = 0.01V_3$ vs t/V_3 . Inset: the distribution of K_i for $L = 12$ in the solid phase. The thick line is 0.24 and the thin line is 0.07.

Fig.4 gives a picture of such an order, in which the local kinetic energy in unit of t is much higher on the half filled bonds than the fully filled ones.

The phase diagrams (Fig.2), derived from both the semi-classical approximation and SSE calculations, matching well, proves the validity of the semi-classical approximation for such a model. However, unlike a model with the nearest neighbor repulsive bosons, neither the $1/3$ filling solid nor the supersolid is found. The supersolid is in fact the superfluid of the hole (particle) excitations on the backbone constructed by particles (holes). Because the bosons are of the hard core, the excited particle can not hop to the nearest site to have the long range off-diagonal order. Meanwhile, due to the domain wall formation¹⁵, the solid order can be destroyed by the infinitesimal density but infinite number of hole excitations, and the phase transition from the solid to the superfluid is allowed.

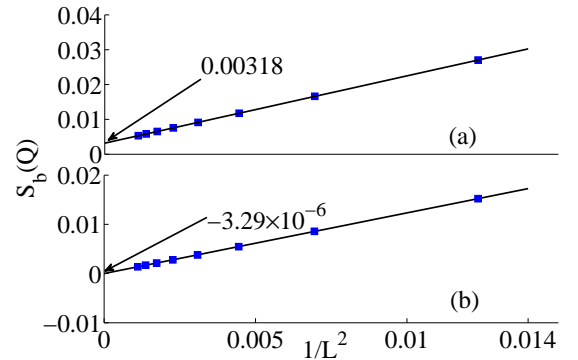


FIG. 5: (Color online) The finite size scaling of $S_b(\mathbf{Q})$. (a) In the solid phase at $\mu/V_3 = 3.5$ and $t/V_3 = 0.36$. (b) In the superfluid phase at $\mu/V_3 = 3.5$ and $t/V_3 = 1$.

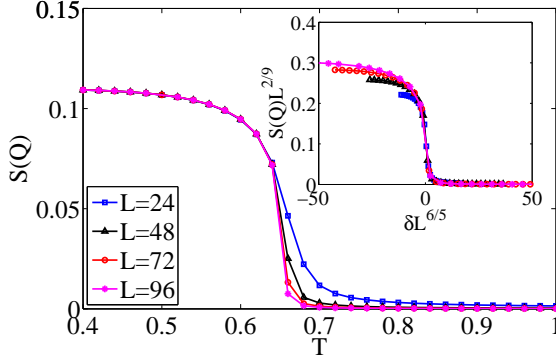


FIG. 6: (Color online) The structure factor vs temperature for different sizes at $t/V_3 = 0.1$ and $\mu/V_3 = 3$. Inset: the critical behavior of the 3-states Potts Model universality class and $\delta = (T - T_c)/t$ with $T_c = 0.65$.

C. Finite Temperature

In the following, we study the finite temperature behaviors in the solid and superfluid phases. In Fig.6, we show the thermal melting process of the CDW order. As the hard-core bosons with only nearest neighbor interactions on the triangular lattice¹⁶, the phase transition is expected to be in the universality class of the 3-state Potts model with the critical exponents $\nu = 5/6$ and $\beta = 1/9$. The critical behavior of the structure factor is $S(\mathbf{Q}) = f(\delta L^{1/\nu}) \times L^{-2\beta}$, where $\delta = (T - T_c)/t$ and T_c is the fitting critical temperature. The Fig.6 shows the phase transition happens in the critical point $T_c = 0.65$ and also confirms our expectation by the same function f for different lattice sizes.

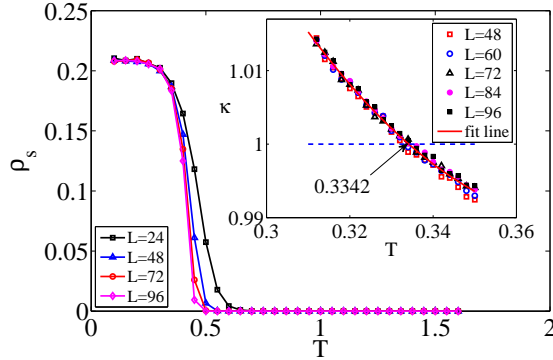


FIG. 7: (Color online) The superfluid density vs temperature for different sizes at $t/V_3 = 0.4$ and $\mu/V_3 = 3.5$. Inset: The solution of the Eq.(5) and the dash line is $\kappa = 1$.

The superfluid to the normal liquid undergoes the Kosterlitz-Thouless transition. The critical temperature can be determined by the renormalization flow and the universal jump of the superfluid density at T_c (Fig. 7). The critical point is given by finding $\kappa = 1$, where $\kappa(T)$

is the integral function

$$4 \ln(L_2/L_1) = \int_{R_2}^{R_1} \frac{dt}{t^2(\ln(t) - \kappa) + t} \quad (5)$$

and $R = 3\pi\rho_s/2tT$. We set data of $L = 24$ as R_1 and the other sizes as R_2 , and then plot the κ in the inset of the Fig.7. From the Fig.7, we observe that the critical point is around $T_c \approx 0.4$. And the inset shows the Kosterlitz-Thouless transition happens at $T_c = 0.3342$.

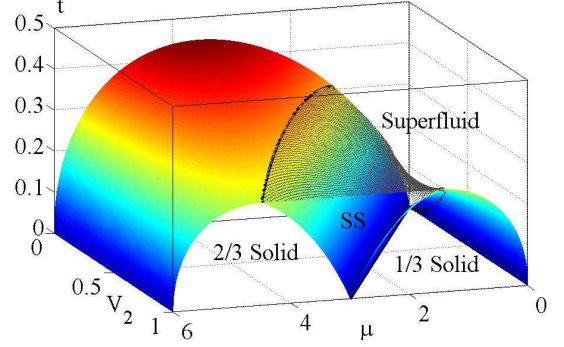


FIG. 8: (Color online) The phase diagram by SCA with $V_2 + V_3 = 1$. The solid phases are under the color surface, the supersolid (SS) exists between the black net and the color surface, and the rest part is the superfluid. The black lines are the tricritical lines.

III. INFLUENCE ON THE SYSTEM WITH NEAREST NEIGHBOR INTERACTION

In the system with only the nearest neighbor interaction, the 1/3 filling solid and supersolid phase¹⁴⁻¹⁶ can stably exist. It is intuitively thought that the additional three-body interactions should have more influences on the 2/3 CDW order than 1/3. By using the semi-classical approximation and setting $V_2 + V_3 = 1$, we plot the phase diagrams for different ratios of V_2 and V_3 in Fig.8. We find that the three-body repulsion strongly enhances the 2/3 CDW order, and the 1/3 CDW order will disappear when V_2 is 0 which indicates that the 1/3 CDW order is associated with the nearest neighbor interaction.

The strong-coupling expansion is powerful on solving the compressible-incompressible second order phase transition. Therefore, we apply it to the supersolid-solid and Mott-superfluid phase transitions. The critical line for Mott-1(Mott-0) insulator-superfluid phase transition is $\mu = 6(V_2 + V_3) + 6t$ ($\mu = -6t$), and the 1/3 and 2/3 supersolid-solid phase transition boundaries are given by

$$\mu_{1/3} = 3V_2 - 3t - \frac{12t^2}{2V_2 + V_3} - \frac{15t^2}{2V_2} - \frac{3t^2}{3V_2 + 2V_3} - \frac{60t^3}{V_2(2V_2 + V_3)} - \frac{9t^3}{V_2(3V_2 + 2V_3)} + \frac{9t^3}{(3V_2 + 2V_3)^2}$$

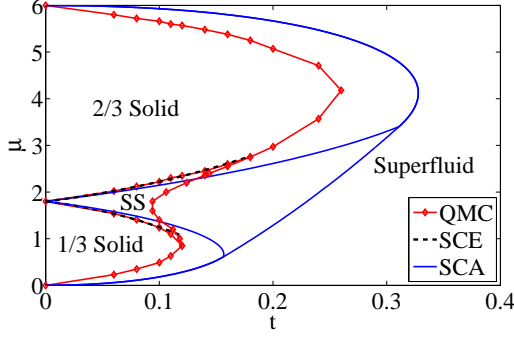


FIG. 9: (Color online) The phase diagrams at $V_2 = 0.6$ and $V_3 = 0.4$ by using the QMC (red dot), SCA (blue line) and strong-coupling expansion(SCE) (black dash line).

$$+ \frac{36t^3}{(2V_2 + V_3)^2} + \frac{15t^3}{4V_2^2} \quad (6)$$

and

$$\begin{aligned} \mu_{2/3} = & 3V_2 + 3t + \frac{12t^2}{2V_2 + 3V_3} + \frac{15t^2}{2V_2 + 4V_3} + \frac{3t^2}{3V_2 + 4V_3} \\ & + \frac{60t^3}{(V_2 + 2V_3)(2V_2 + 3V_3)} + \frac{9t^3}{(V_2 + 2V_3)(3V_2 + 4V_3)} \\ & - \frac{9t^3}{(3V_2 + 4V_3)^2} - \frac{36t^3}{(2V_2 + 3V_3)^2} - \frac{15t^3}{4(V_2 + 2V_3)^2}. \end{aligned} \quad (7)$$

When V_3 goes to the infinity, the Mott-1 insulator will disappear and the first order phase transition line given by $\mu_{2/3}$ disappears. In contrary, the $\mu_{1/3}$ is partly affected in this limit and the Mott-0 insulator-superfluid critical line is not changed. Furthermore, these critical lines are compared with results from the quantum Monte Carlo and semi-classical approximation at $V_2 = 0.6$ and $V_3 = 0.4$ in Fig.9. We see again that the semi-classical approximation gives a qualitative matched phase diagram to that comes from the quantum Monte Carlo. In the region that the strong-coupling expansion is valid, the results fitting with the data from quantum Monte Carlo are better than those from the semi-classical approximation.

In order to detect the three-body interactions' impacts on the different orders, we use quantum Monte Carlo to simulate several variables. In terms of the Fig.10, we can find, comparing to the 1/3 solid phase which hardly affected by the three-body repulsion, the 2/3 filling CDW order are strongly enhanced due to decreasing of the local vibrations. In the supersolid phase, the CDW order is also enhanced, but the superfluid order becomes weak at the same time. The influence on the 2/3 supersolid is stronger than that on the 1/3 supersolid, because the repulsive effect is larger in former case on the superfluid flux. It is also interesting that the minima of the superfluid density and the structure factor are separated in the large V_3 . In the Fig.11, we can observe it in the small

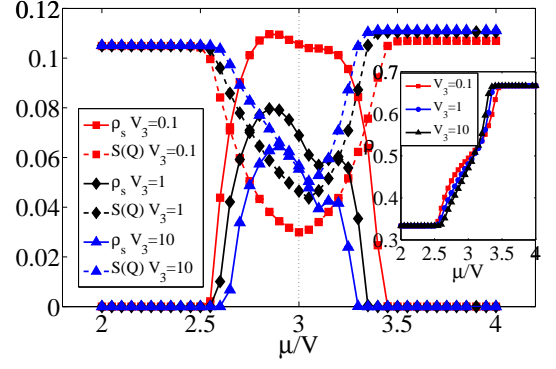


FIG. 10: (Color online) The superfluid density and the structure factor at $T = 0.02$, $L = 24$, $V_2 = 1$ and $t = 0.1$ for different V_3 varying as μ . Inset: The density per site

region. Two possible reasons may be used to interpret it. (i) The minimum of the $S(\mathbf{Q})$ determines the 1/3-2/3 supersolid phase transition, because the competition between both orders in the critical line may minimize the $S(\mathbf{Q})$. (ii) Because the second order hopping process in the 2/3 supersolid are partly prohibited by the three-body interactions, the holes moving on the honeycomb backbone constructed by the particles can be approximately treated as, the quasi-particles forming the superfluid flux on the honeycomb lattice. For the same reason mentioned in the Ref.^{27,28}, such dip indicates the geometric hindrance in the superfluid flow.

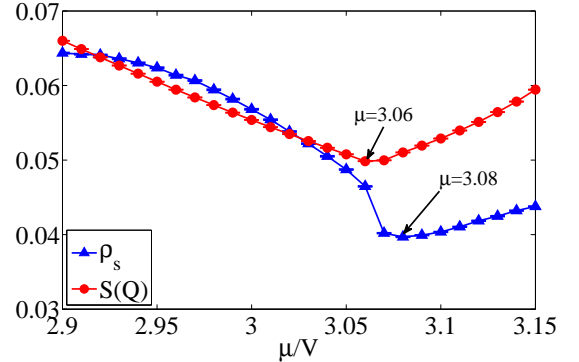


FIG. 11: (Color online) The superfluid density (blue) and the structure factor (red) in small region at $T = 0.01$, $L = 24$, $V_2 = 1$ and $t = 0.1$ for $V_3 = 10$ by varying the μ .

IV. CONCLUSION

We studied the hard-core Bose-Hubbard Model with nearest neighbor and three-body repulsions on the triangular lattice by using the semi-classical approximation and the Quantum Monte Carlo simulation. In the only three-body repulsions case, we got the complete phase

diagram and find no $1/3$ solid and supersolid phase exist. By comparing with the CDW and BOW order, we demonstrate they coexist in the solid phase and the BOW order trivial results from the local vibrations, so it enlighten us it needs to be more careful to judge the BOW+CDW order. At the finite temperature, the superfluid phase changes into the normal liquid phase after a Kosterlitz-Thouless transition. Meanwhile, the 3-state Potts Model universality class phase transition emerges when heating up the solid state. And these thermal properties are same as the solid phase in the system with only nearest neighbor interaction¹⁶.

After adding the nearest neighbor repulsion, the supersolid and $1/3$ solid phase revive. The three-body repulsions can enhance the $2/3$ CDW order and suppress the high order hopping, so they affect the phase with $2/3$ CDW order harder than $1/3$ CDW order. However, even up to infinity, it still can not destroy the $2/3$ supersolid, because the excited holes in the honeycomb backbone constructed by the particles in two sublattices still

can form the superfluid flow without feeling the three-body repulsions. For the large V_3 , the minima of the superfluid and CDW order are separated. The dip of the CDW order may indicate the first order $1/3$ - $2/3$ SS phase transition¹⁶, and the dip of superfluid density may result from the geometry hindrance.

V. ACKNOWLEDGEMENT

The authors would like to thank for discussions with S.Eggert and his suggestions. XFZ thanks the members of SFB/TRR 49. This work is supported by the National Natural Science Foundation of China, the national program for basic research of MOST of China, the Key Lab of Frontiers in Theoretical Physics of CAS, the Natural Science Foundation of Beijing under Grant No.1092009, the DAAD, and the DFG via the Research Center Transregio 49.

-
- * Electronic address: zxf@itp.ac.cn
- ¹ Special Issue on Ultracold Polar Molecules: Formation and Collisions, Eur. Phys. J. D. **31** (2004).
 - ² A. Micheli, G. K. Brennen and P. Zoller, Nature Physics **2**, 341 (2006)
 - ³ D. Jaksch and P. Zoller, Ann. Phys. **315**, 52 (2005).
 - ⁴ M.A.Levin and X.G.Wen, Phys. Rev. B **71**, 045110 (2005)
 - ⁵ A.W.Sandvik, S. Daul, R. R. P. Singh and D. J. Scalapino Phys. Rev. Lett. **89**, 247201 (2002).
 - ⁶ R.G.Melko, A.W.Sandvik and D.J.Scalapino, Phys. Rev. B **69**, 100408(R) (2004).
 - ⁷ R.G.Melko and A.W.Sandvik, Phys. Rev. E **72**, 026702 (2005)
 - ⁸ H.P.Büchler, A.Micheli and P.Zoller, Nature Physics **3**, 726 (2007)
 - ⁹ B.Capogrosso-Sansone S. Wessel, H. P. Büchler, P. Zoller, and G. Pupillo, Phys. Rev. B **79**, 020503(R) (2009)
 - ¹⁰ K. P.Schmidt, J. Dorier and A. M. Läuchli, Phys. Rev. Lett. **101**, 150405 (2008)
 - ¹¹ L. Bonnes, H. P. Büchler, and S. Wessel, New J. Phys. **12**, 053027 (2010)
 - ¹² J.K. Pachos and M.B. Plenio, Phys. Rev. Lett. **93**, 056402 (2004)
 - ¹³ Y. Shimizu, K. Miyagawa, K. Kanoda, M. Maesato, and G. Saito Phys. Rev. Lett. **91**, 107001 (2003)
 - ¹⁴ G. Murthy, D. Arovas, and A. Auerbach, Phys. Rev. B **55**, 3104 (1997).
 - ¹⁵ S. Wessel and M. Troyer, Phys. Rev. Lett. **95**, 127205 (2005); D. Heidarian and K. Damle, Phys. Rev. Lett. **95**, 127206 (2005). R.G. Melko A. Paramekanti, A. A. Burkov, A. Vishwanath, D. N. Sheng, and L. Balents, Phys. Rev. Lett. **95**, 127207 (2005).
 - ¹⁶ M. Boninsegni and N. Prokof'ev, Phys. Rev. Lett. **95**, 237204 (2005).
 - ¹⁷ A. Sen, P. Dutt, K. Damle, and R. Moessner, Phys. Rev. Lett. **100**, 147204 (2008).
 - ¹⁸ F. Wang, F. Pollmann, and A. Vishwanath, Phys. Rev. Lett. **102**, 017203 (2009).
 - ¹⁹ H.C. Jiang M. Q. Weng, Z. Y. Weng, D. N. Sheng, and L. Balents, Phys. Rev. B **79**, 020409(R) (2009).
 - ²⁰ D. Heidarian and A. Paramekanti, Phys. Rev. Lett. **104**, 015301 (2010).
 - ²¹ L.Pollet, J.D.Picon, H.P.Büchler and M.Troyer, Phys. Rev. Lett. **104**, 125302 (2010)
 - ²² A.Eckardt P. Hauke, P. Soltan-Panahi, C. Becker, K. Sengstock and M. Lewenstein, EPL **89**, 10010 (2010)
 - ²³ C.Becker P. Soltan-Panahi, J. Kronjäger, S. Dörscher, K. Bongs, K. Sengstock, New J. Phys. **12**, 065025 (2010)
 - ²⁴ A.W. Sandvik, Phys. Rev. B **59**, R14157 (1999);
 - ²⁵ O.F. Syljuåsen and A.W. Sandvik, Phys. Rev. E **66**, 046701 (2002).
 - ²⁶ K. Louis and C. Gros, Phys. Rev. B **70**, 100410(R) (2004)
 - ²⁷ Stefan Wessel, Phys. Rev. B **75**, 174301 (2007)
 - ²⁸ J. Y. Gan, Yu Chuan Wen, Jinwu Ye, Tao Li, Shi-Jie Yang, and Yue Yu, Phys. Rev. B **75**, 214509 (2007)